

Pulsed magnetic fields at the ESRF

First results

*F. Duc, P. Frings, J. Vanacken, C. Detlefs, J.E. Lorenzo,
M. Nardone, J. Billette, A. Zitouni, W. Bras, and G.L.J.A. Rikken*

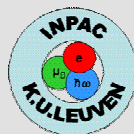
Laboratoire National des Champs Magnétiques Pulsés, Toulouse, France

Pulsveldengroep, INPAC, Leuven, Belgium

ESRF, Grenoble, France

Laboratoire de Cristallographie, Grenoble, France

DUBBLE CRG @ ESRF, Grenoble, France



- Motivations
- Experimental set-up
 - Pulsed field & cryogenics (LNCMP)
 - ESRF beamline and detector
- Integration of both techniques
- First results on TbVO_4
- Future developments and applications

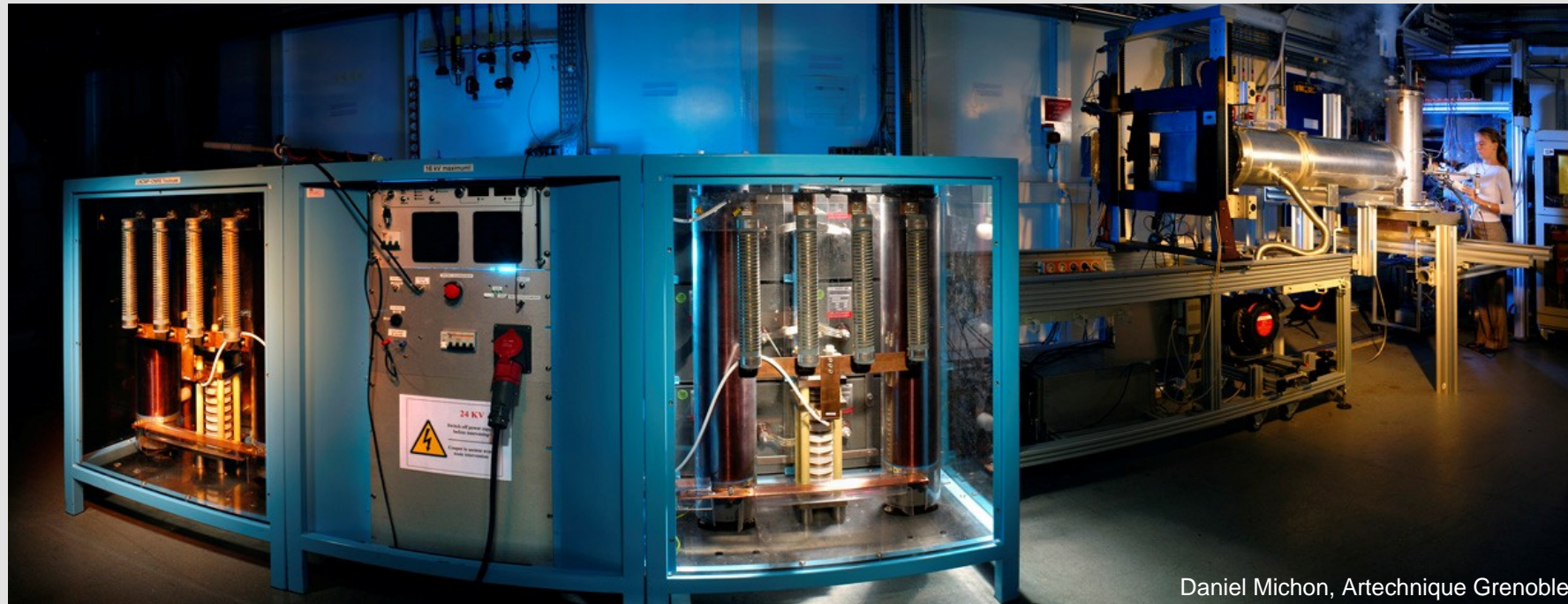
- Magnetic field is a thermodynamic variable of fundamental importance
It is one of the important external parameters, such as T , P and E , which control phase transitions.
- **Studies in high magnetic fields** of systems with quantum correlations effects are of fundamental interest
 - to lift the degeneracy of degenerate quantum states (Zeeman effect)
 - to select quantum states
 - to break up of strong correlations between electrons (magnetism, superconductivity)
- All of the current high field measuring techniques are macroscopic (M , χ , r , V_H , C_v , v_s, \dots)...
...Until recently, there was no direct information on the structural properties above 15 T. Whereas we know (from low field measurements) that often field-induced phase transition do have a structural component.
- Sound velocity v_s and dilatometry at high fields also indicate structural effects.

 **Combination of X-ray techniques with High Magnetic Fields**

The Pulsed Field generator



Mobility of pulsed fields equipment

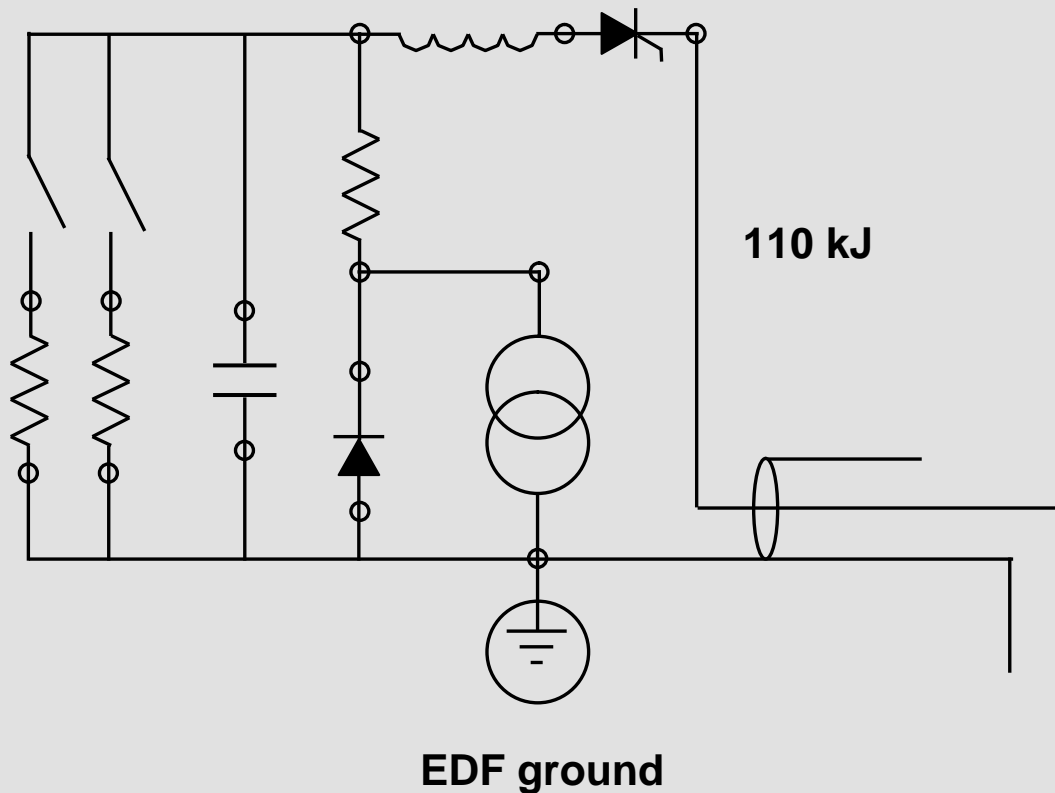


Daniel Michon, Artechnique Grenoble

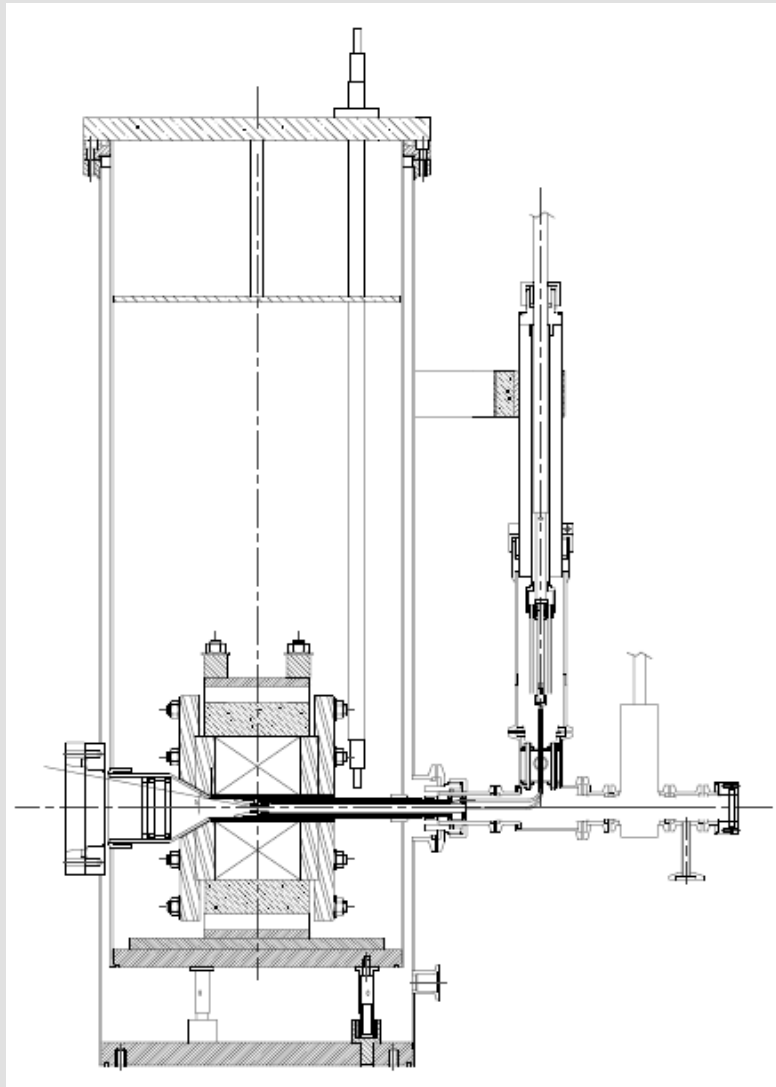
Generator (LNCMP capacitor bank)

- Three subunits:
 - 2 storage units contain: capacitors, crowbar diodes and resistors, and current limiters.
 - Control unit houses: charger, thyristor stack, dump resistors and relays, I-V monitors.
- 130 kJ. 16 kV
- The combined weight of the generator is 2800kg and dimensions are 1.25 x 1.3 x 2.85 m³.

capacitor bank (16 kV)



- Max energy: 130 kJ
- $V_{\max} = 16$ kV
- $C = 1$ mF (12 x 0.083 mF)
- $R_{\text{crowbar}} = 225$ m Ω
- $L_{\text{prot}} = 0.25$ mH (17.5 m Ω)
- $I_{\text{short}} = 48$ kA (0.8ms)
- Optically triggered thyristor switch
- $R_{\text{dump1}} = 1$ k Ω
- $R_{\text{dump2}} = 1$ k Ω



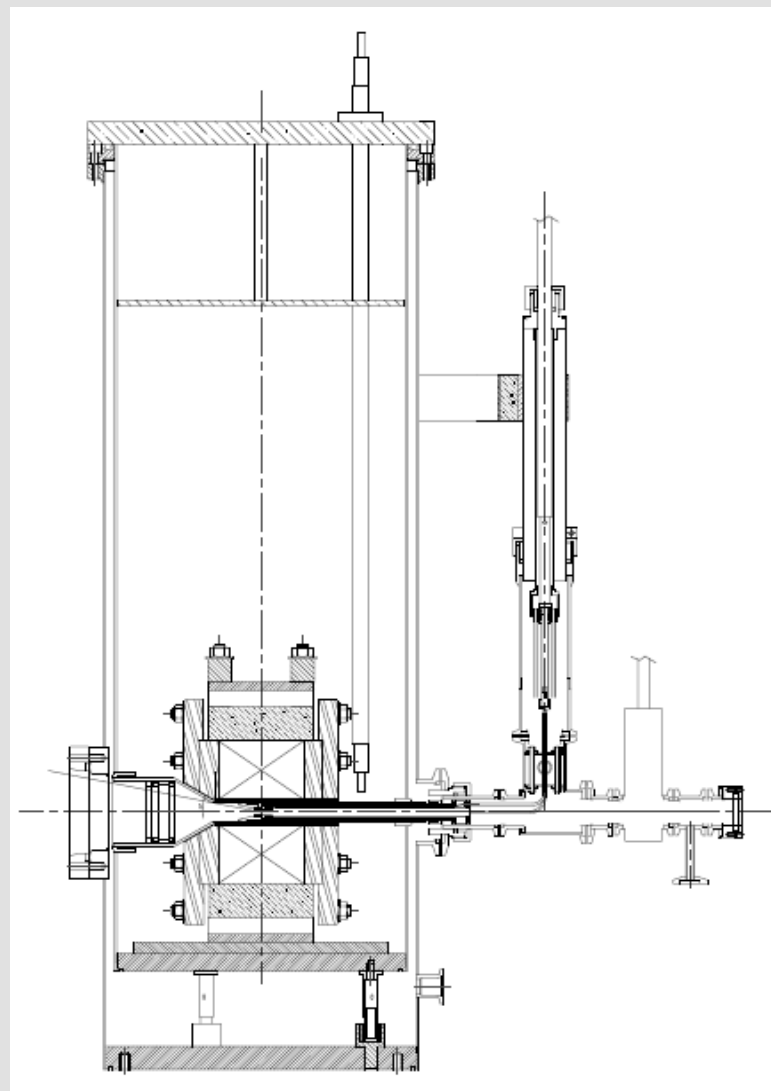
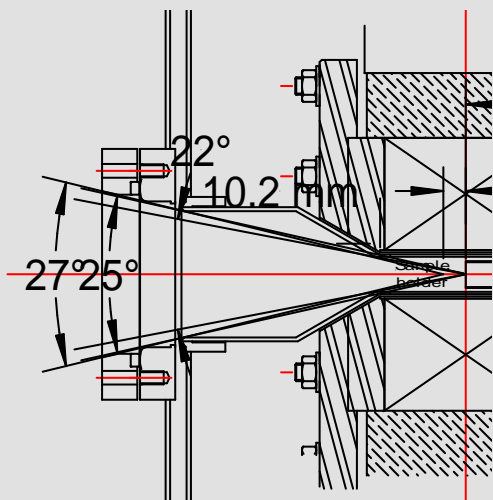
High field magnet (LNCMP)

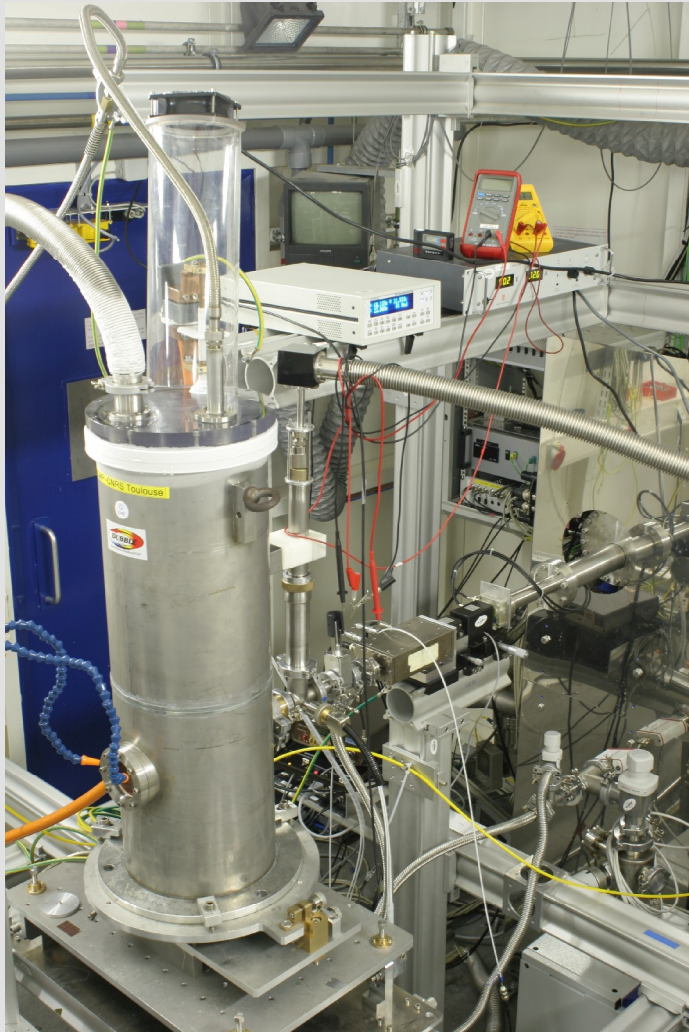
- coil is wound of Glidcop wire
- bore of 20 mm \varnothing , external $\varnothing = 124$ mm, height = 74 mm
- $L(T=77K) = 8.63$ mH, $R(T=77K) = 80$ m Ω
- coil is horizontally mounted
- Beam axis was along the bore of the magnet (Faraday geometry)
- magnet immersed in liquid nitrogen



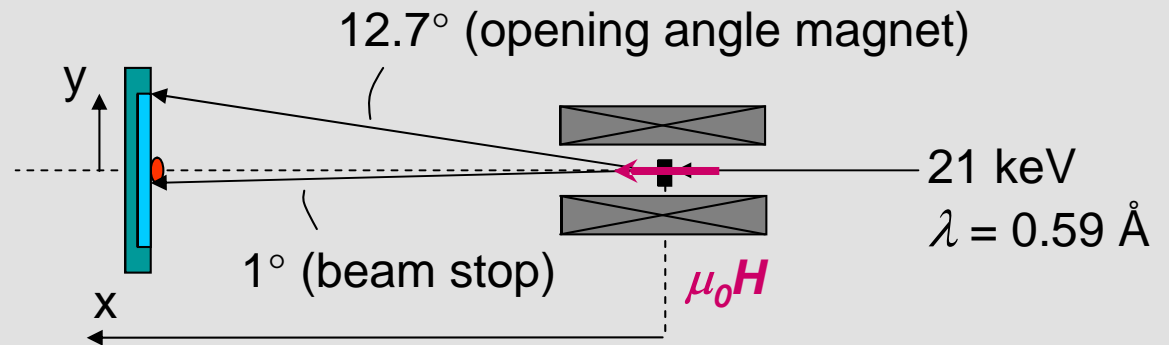
Sample cryostat (LNCMP)

- He flow system
- ~7 K to 300 K
- PID heater control
- T-sensors (2)
- dB/dt sensor (Field)
- Fits inside magnet
- allows bundle to pass
- sample top-loading !



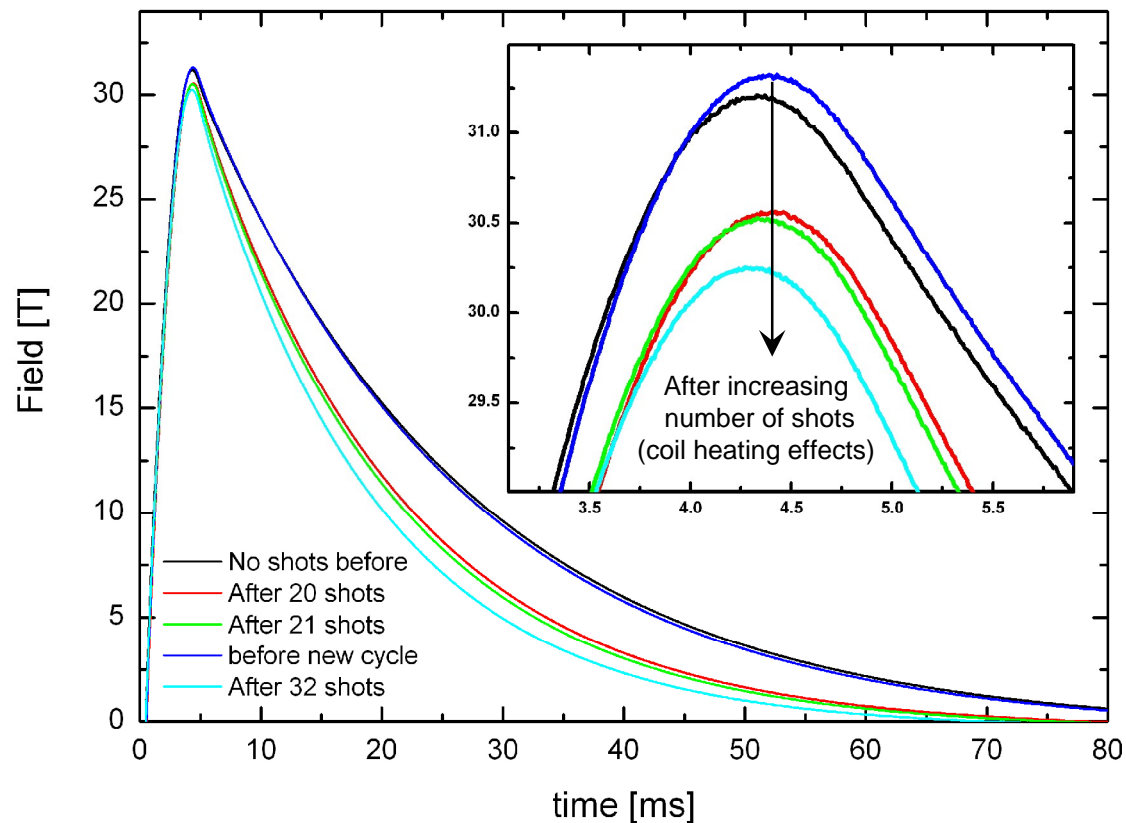


- Limited opening angle cryostat/magnet : $\sim 13^\circ$



$$\left. \begin{aligned} 2d \sin \theta &= \lambda \\ d &= 2\pi / Q \end{aligned} \right\}$$

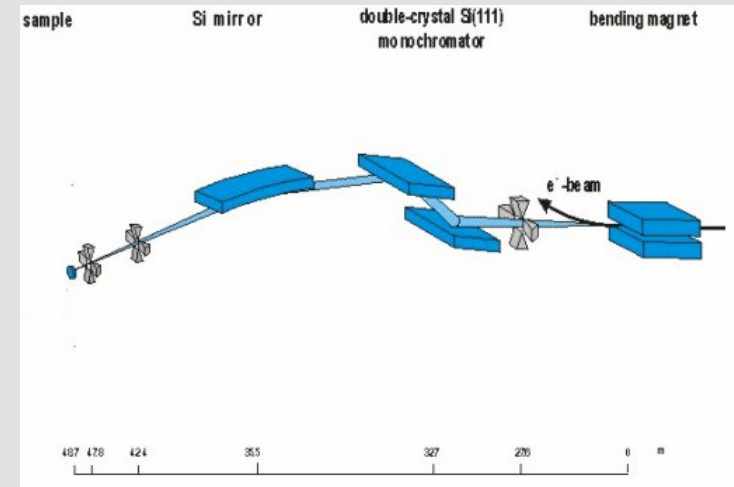
⇒ Restriction of the available Q-space to 2.4 \AA^{-1}



Magnetic field **up to 30 T** (110 kJ. 16 kV)

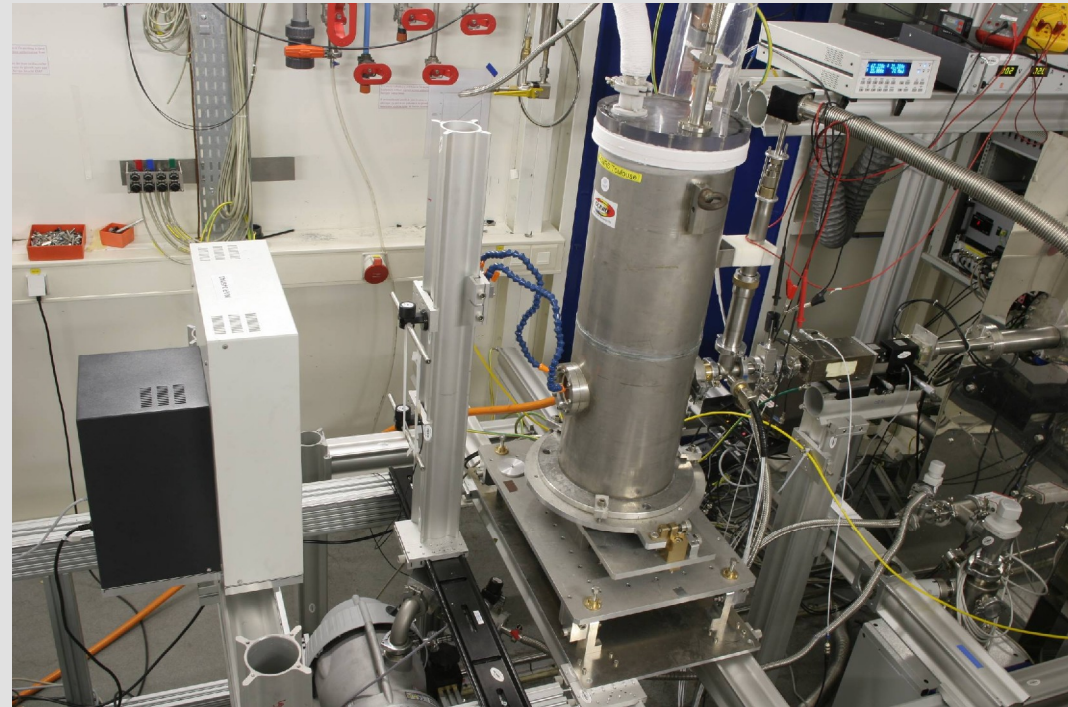
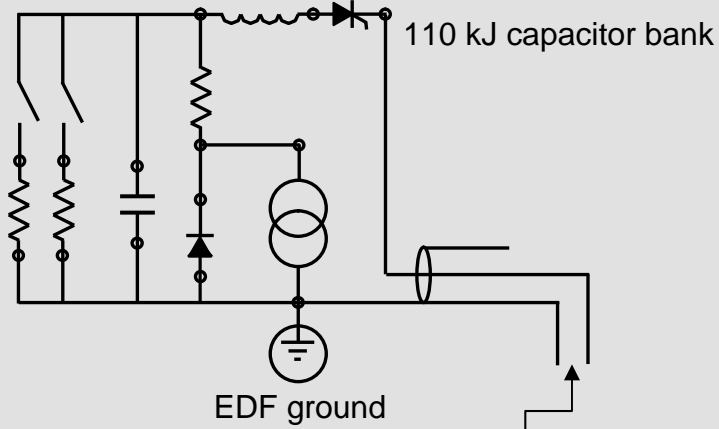
DUBBLE CRG-Beamline (BM26B, ESRF)

- Photons emitted from the 0.8T bending magnet
- Monochromatized by a Si(111) double crystal monochromator tuned to 21 keV ($\lambda = 0.59 \text{ \AA}$)



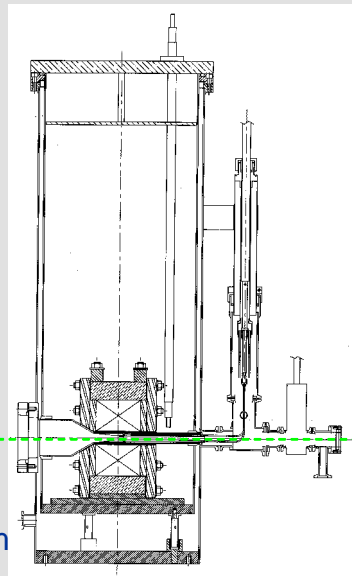
ESRF detector

- on-line image plate (MAR345)
- resolution of the plate : 100 μm /pixels
- detector area: 345 mm x 345 mm
- Not time resolved !



LN cooled 30T magnet

Image plate
On-line readout



Beam stop

Flow cryostat

Ionization chamber

Fast shutter

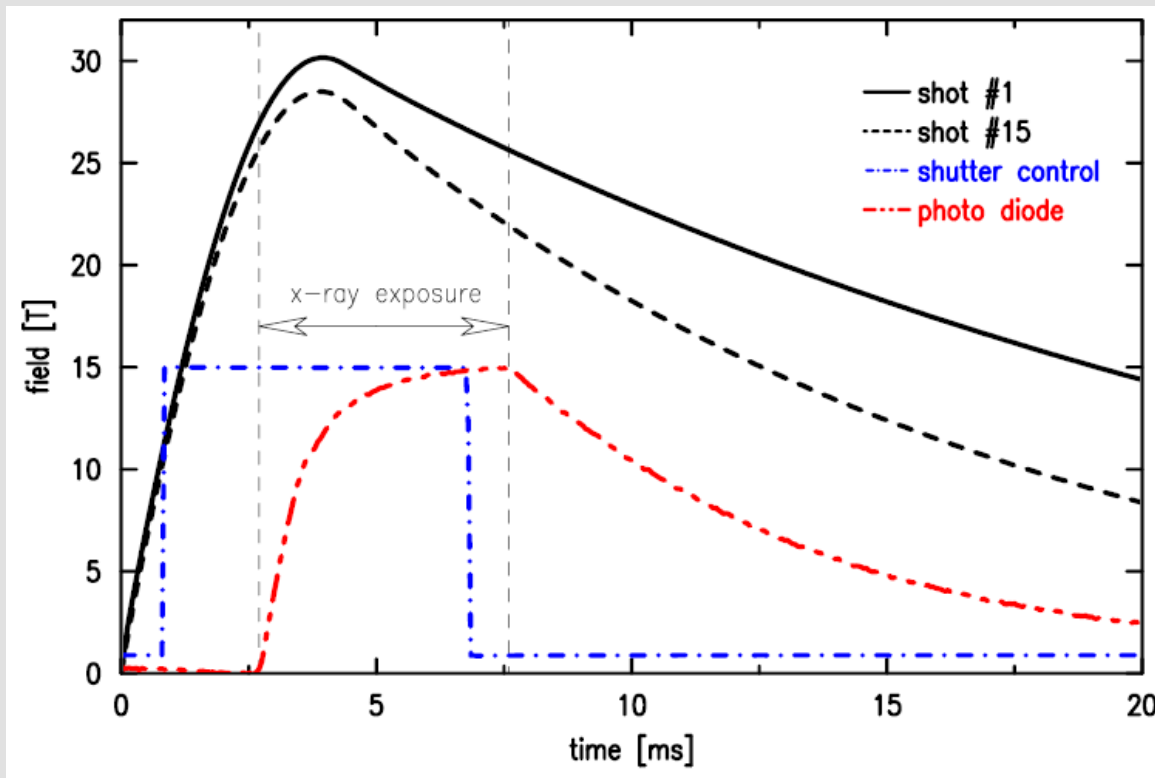
Ionization chamber

Slow shutter



Monochromatic 21keV beam

- The magnetic field pulse and the X-ray shutters are synchronized by a common trigger
- Open/close beam after predefined delays
- Average magnetic field during the exposure is within 90% of its maximum value
- Time frames = 4.9ms
- Accumulation of series of pulses in order to obtain enough diffraction counts in the detector



Data collection at one field :

- **30T** : 15 pulses in 15 min } 1H00
- 45 min of cool down time }
- Real exposure time:
 $\sim 15 \times 5\text{ms} = 75\text{ms}$

TbVO_4 (REXO_4)

- $T_{JT} = 33.1$ K
Cooperative Jahn-Teller transition :
Ordering of the quadrupolar moments of the RE ions

- $T > 33.1$ K
Tetragonal zircon structure $I4_1/amd$ (D_{4h}^{19})

$$a = 7.1841(3) \text{ \AA}$$

$$c = 6.3310(4) \text{ \AA}$$

Site symmetry of Tb^{3+} , $4f^8$: (D_{2d})

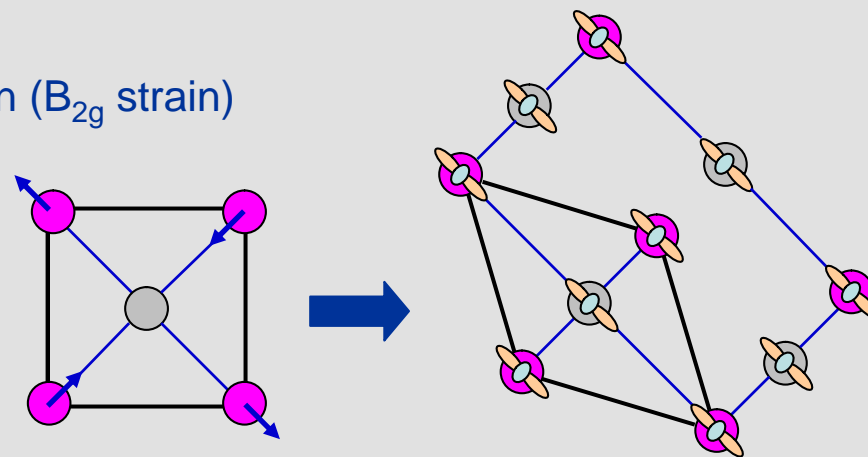
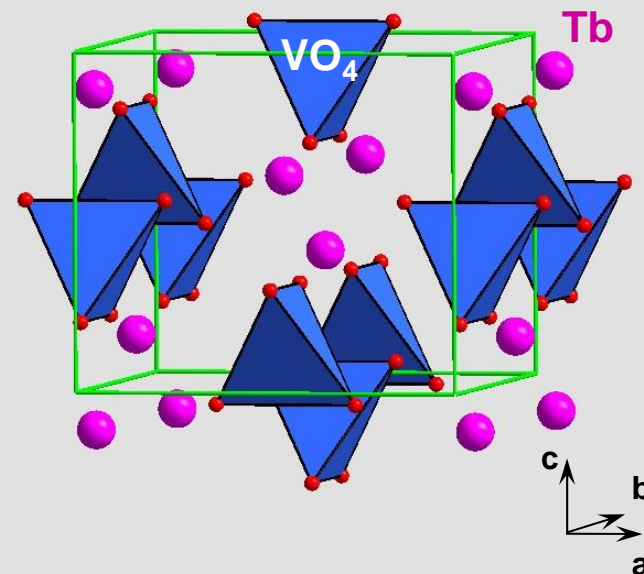
- $T < 33.1$ K
Crystal deformation along the $[110]$ direction (B_{2g} strain)

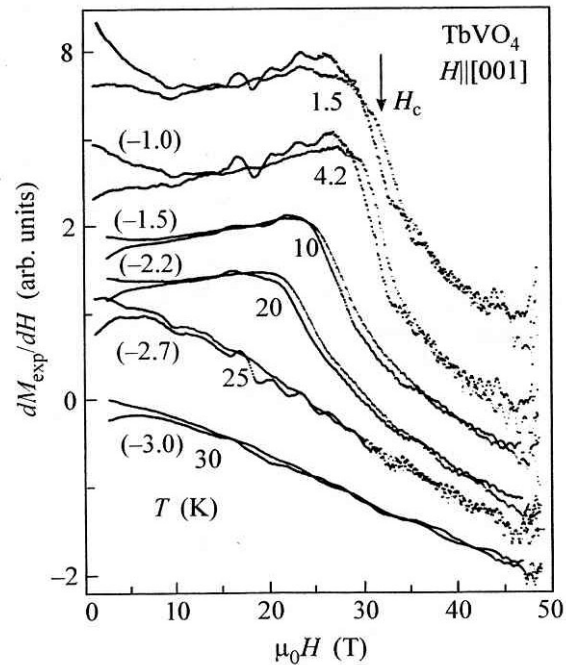
Orthorhombic structure $Fddd$ (D_{2h}^{24})

$$a = 10.239(2) \text{ \AA}$$

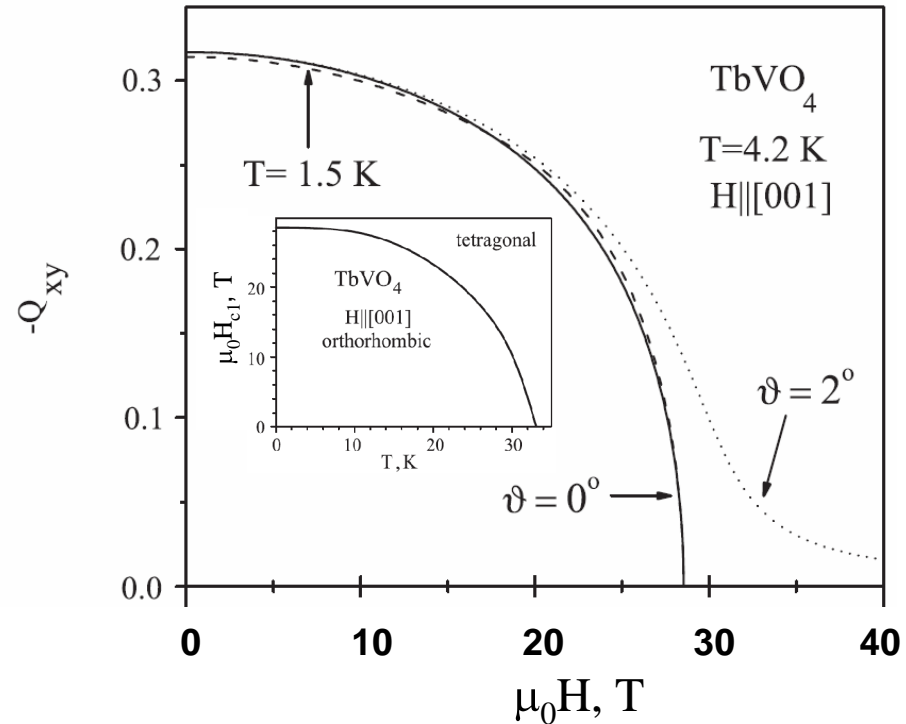
$$b = 10.029(2) \text{ \AA}$$

$$c = 6.315(1) \text{ \AA}$$







Z.A. Kazei et al., *JETP Letters* 82 (2005) 609-612



Demidov et al., *Physica B* 363 (2005) 245-251

Effect of a strong magnetic field $B \parallel [001]$

- Prediction of the destruction of the quadrupolar ordering
-  Suppression of the Jahn-Teller state of TbVO_4 by a field of 29 T
-  Inducing symmetry change from orthorhombic to tetragonal

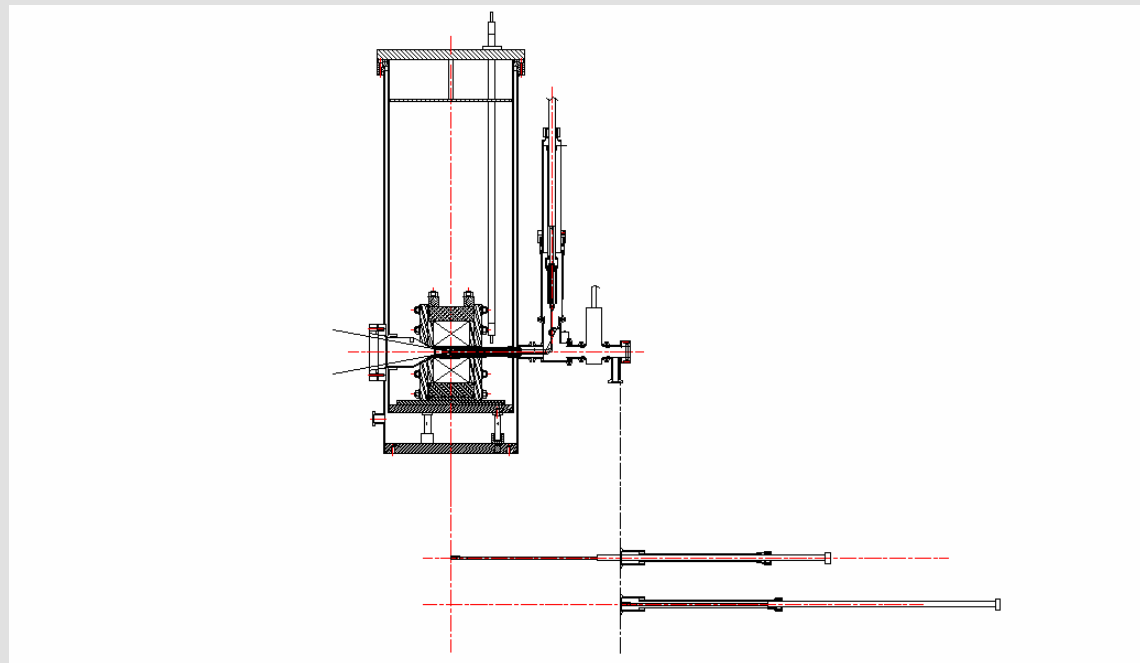
Flux-grown single crystals of TbVO_4 (P.C. Canfield, Ames Lab.), ground into a fine powder

- Random distribution of grain orientations

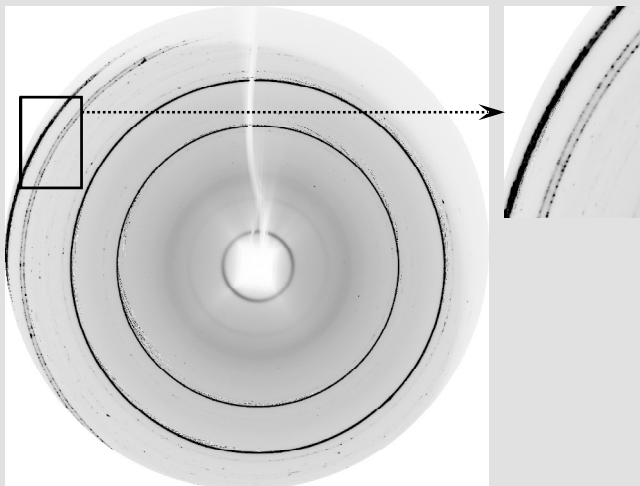
Embedded in a polymer matrix (polyvinylpyrrolidone)

- Reduce movement of the powder grains
- Improve thermal contact

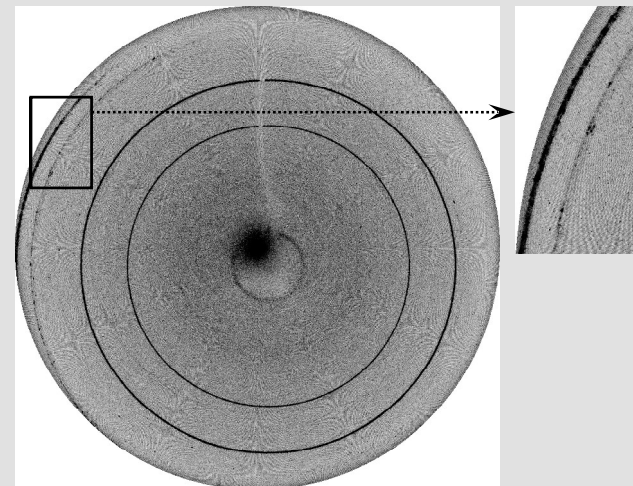
Thickness of the pellets adjusted to limit X-ray absorption (pellets of 4 mm \varnothing)



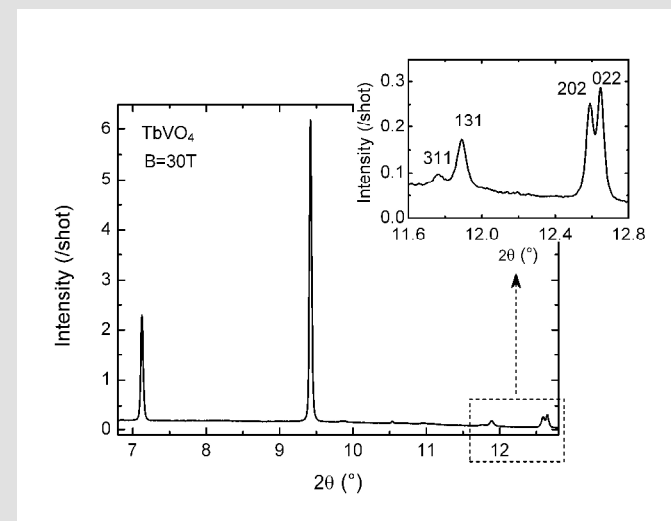
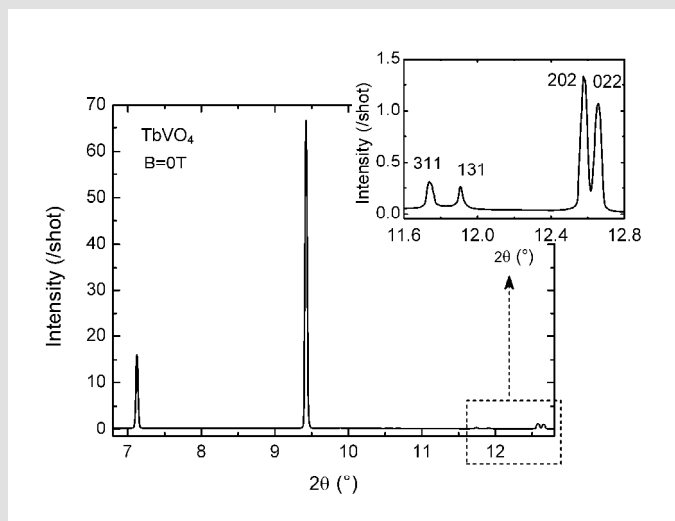
Pulsed field diagrams



$B = 0$ T, $T = 7.5$ K, exposure time : 60s

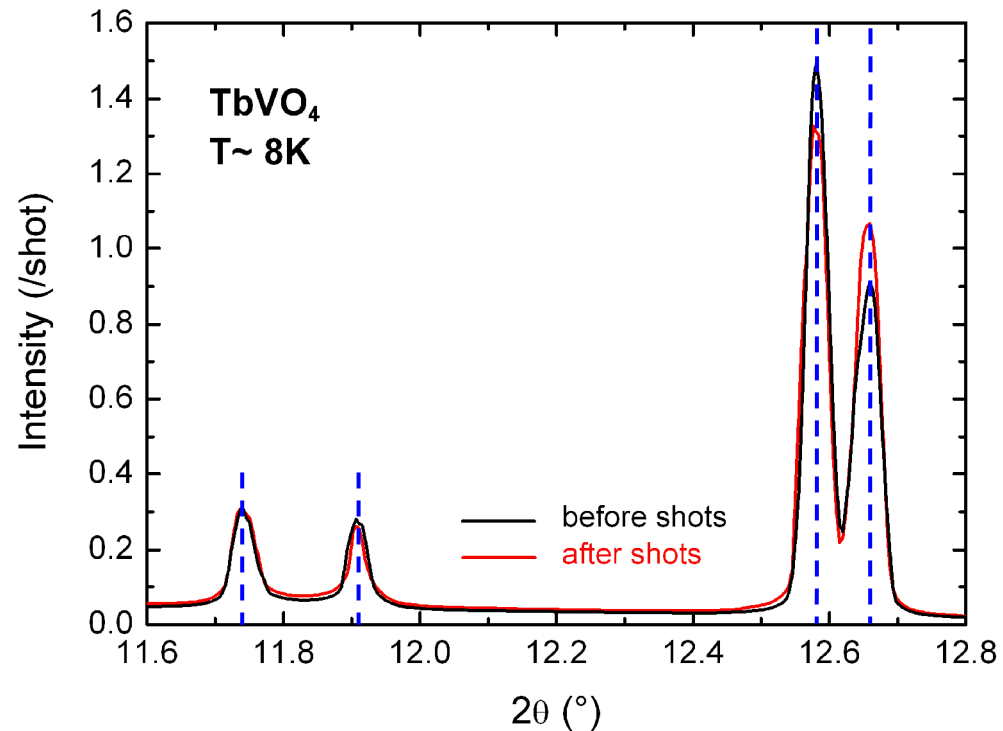


$B = 30$ T, $T = 7.5$ K, exposure time : ~75ms



Data normalized to one shot, i.e. 5ms

- Control of change in distribution by **zero field measurement** before and after applying series of $B = 30$ T magnetic field shots:



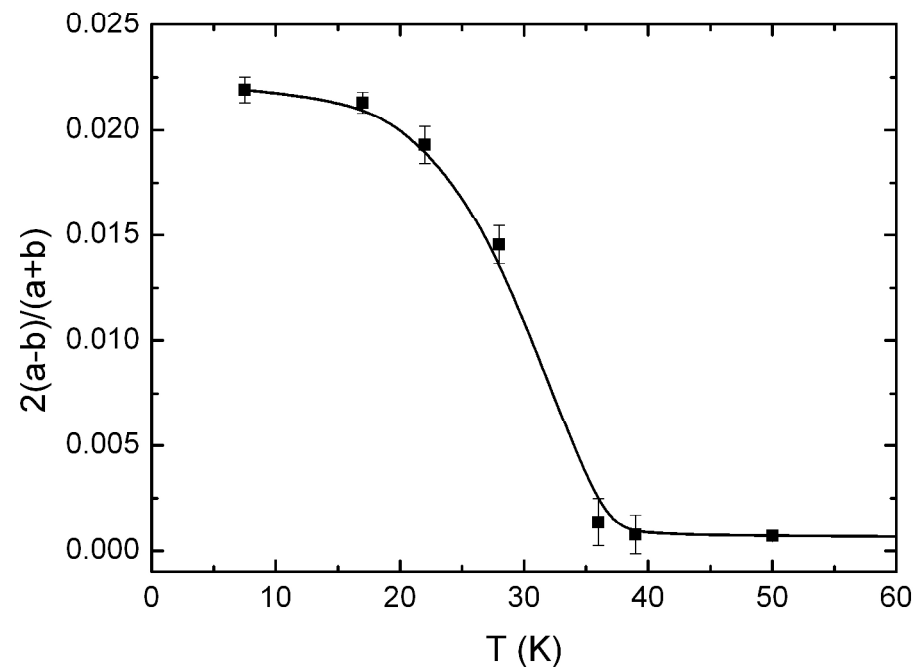
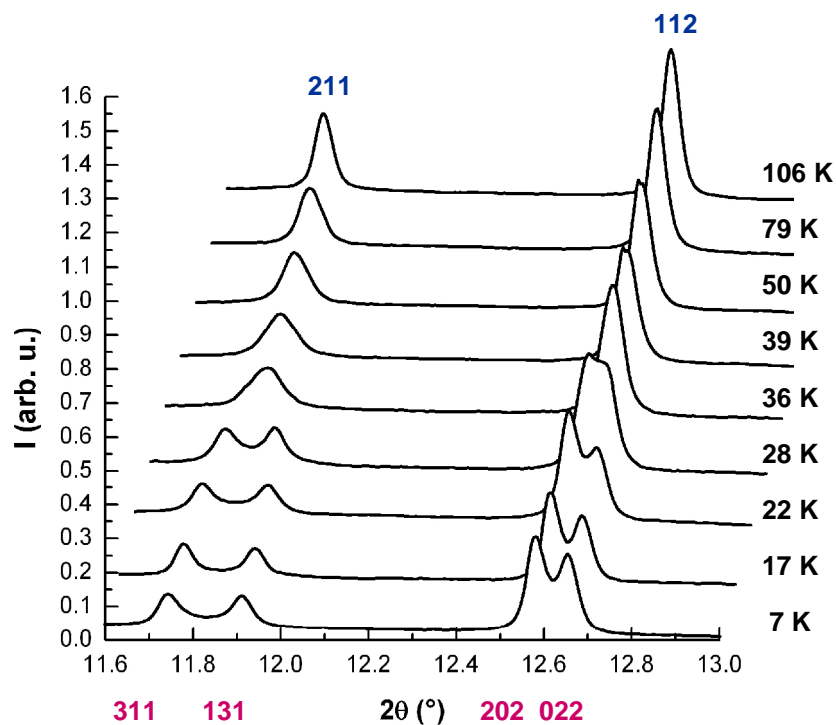
- No shift of diffraction peaks
- Small variation in peak amplitude

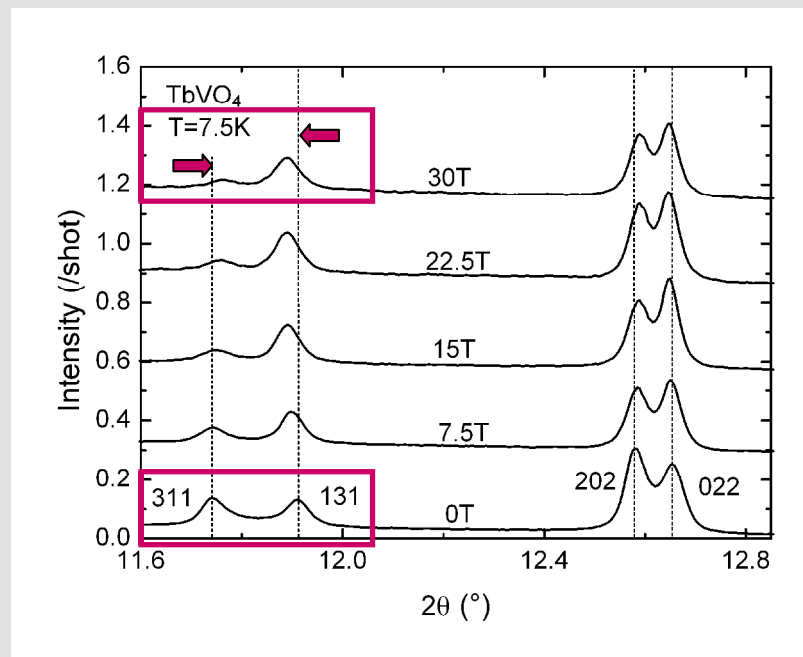
Structural changes with temperature


The Jahn-Teller transition in TbVO_4

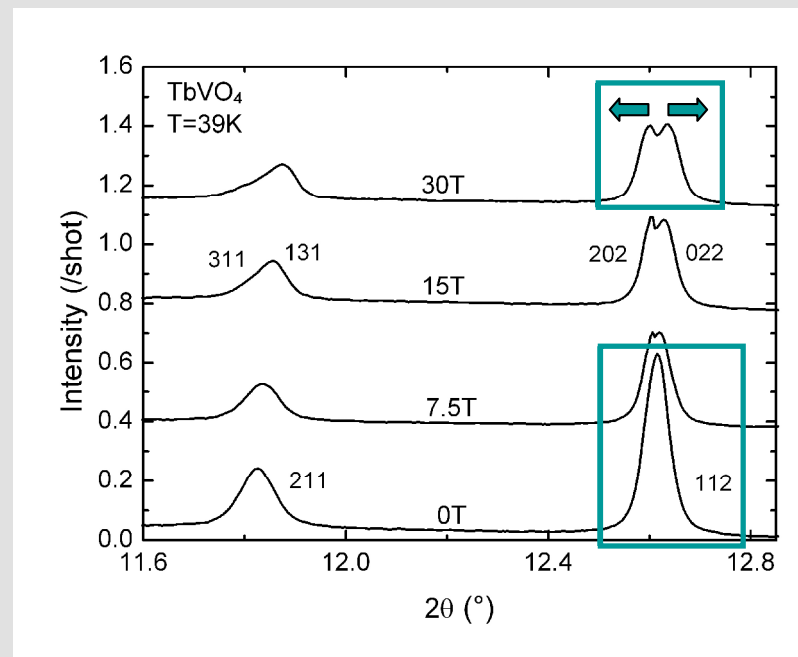
Temperature dependence of diffraction patterns


Orthorhombic distortion

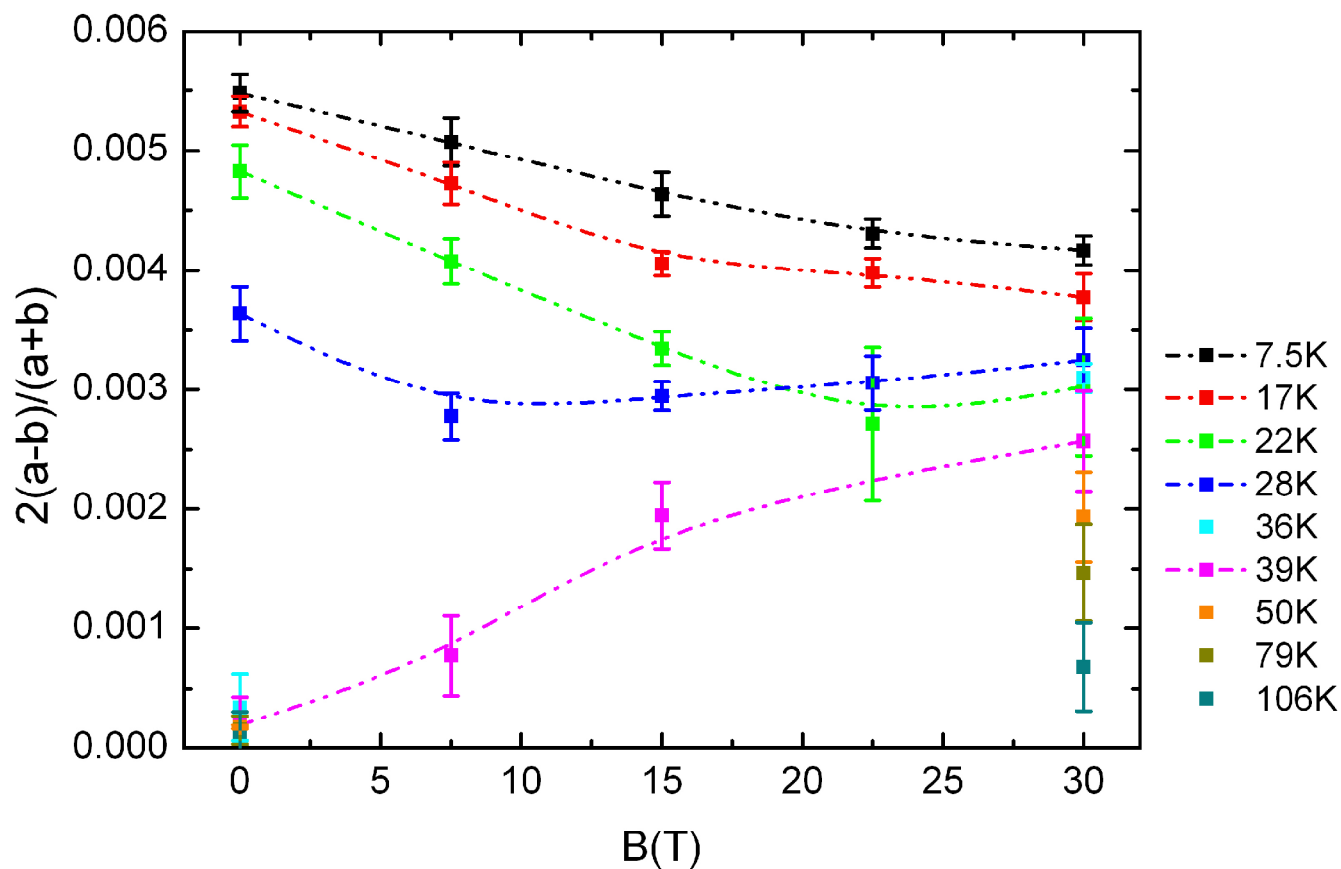




- $B = 0T, T = 7.5 K \rightarrow$ Orthorhombic
 (311) + (131)
 (202) + (022)
- $B \neq 0T, T = 7.5 K$
 Preferential population of domains
 In-plane magneto-crystalline anisotropy
 Splitting decreases with increasing B
 B decreases the ortho. distortion



- $B = 0T, T = 39K \rightarrow$ Tetragonal
 (211)
 (112)
- $B \neq 0T, T = 39K$
 Splitting appears with B
 Preferential domain population
 B induces the ortho. distortion



Orthorhombic distortion as a function of applied field

Quantitative analysis of the data

- Theory:
 - $B // [001]$ suppress the distortion
 - $B // [110]$ enhance the effect
- TbVO_4 : sample with large magneto-crystalline anisotropy
The H - T phase diagram depends on:
 - the magnitude of B
 - the orientation of B relative to the symmetry axes
- X-ray powder diffraction:
 - Direct measure of the Jahn-Teller distortion (lattice parameters, symmetry changes)
 - Random distribution of the powder grains with respect to the external field
 - in some grains the JT-effect is enhanced
 - in others it is suppressed

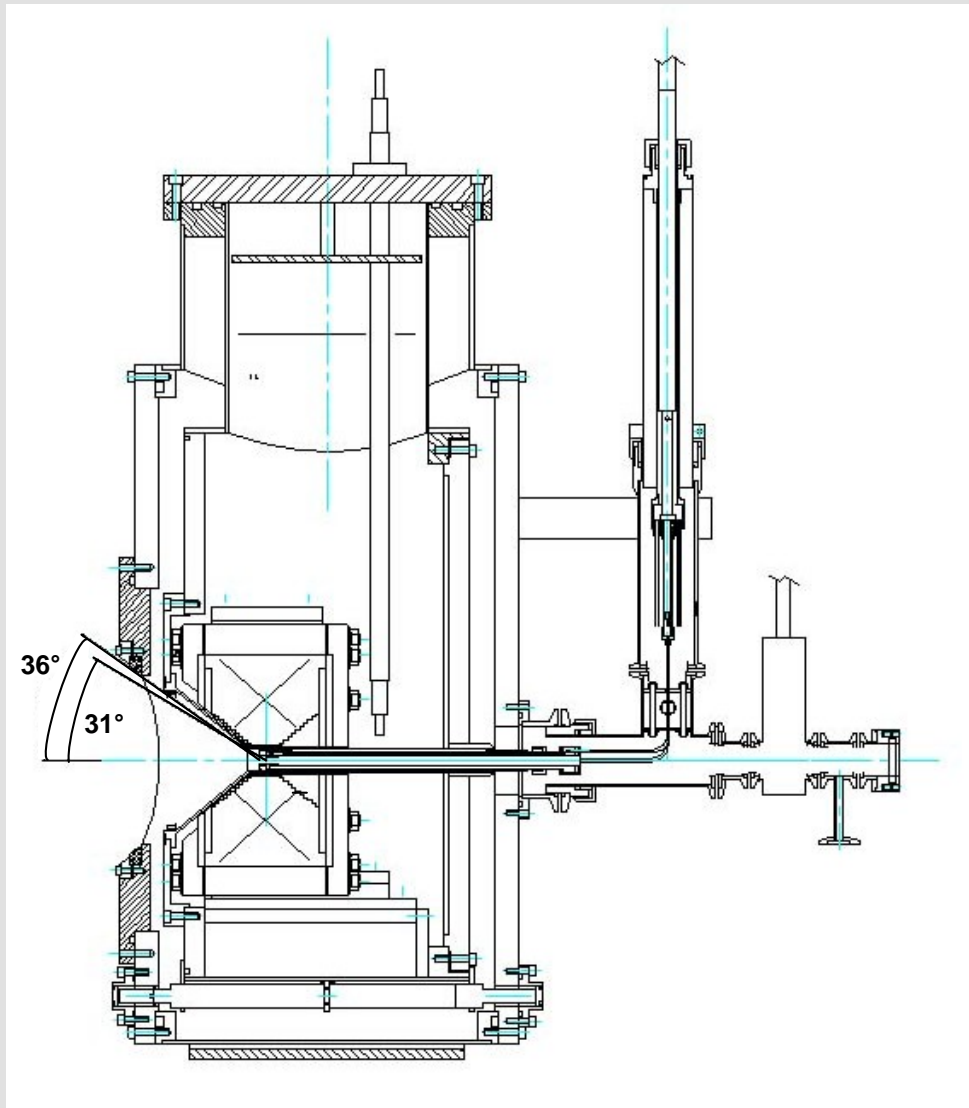
This had to be taken into account in the data analysis

Final goal of the project

Provide the highest magnetic fields possible within the constraints imposed by the synchrotron x-ray beamline

Technological developments

- Higher fields, up to 40 T
- New design of the magnet coil
 - 1) Increase the opening angle of the coil in the Faraday geometry ($B //$ beam)
 - 2) Split pair coil ($B \perp$ beam): wider optical access angles
- Lower temperatures with better temperature control
- Automation of the operation mode
- Longer field pulses to facilitate the synchronization with shutters and detection electronics
- Fast x-ray detector (frame rate of 1 kHz or better)

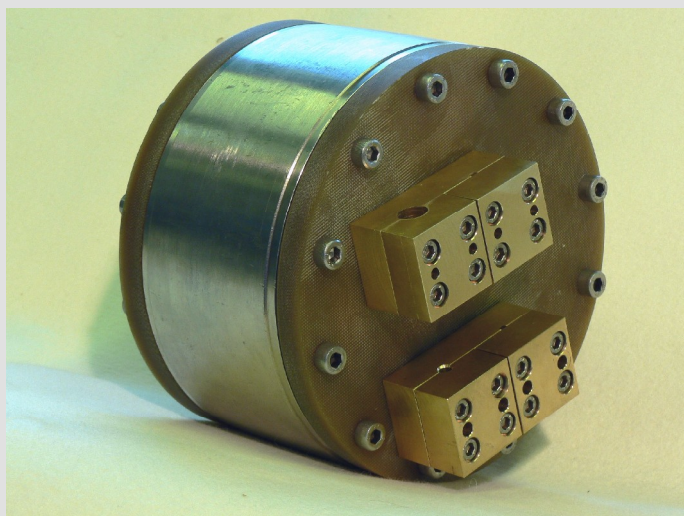
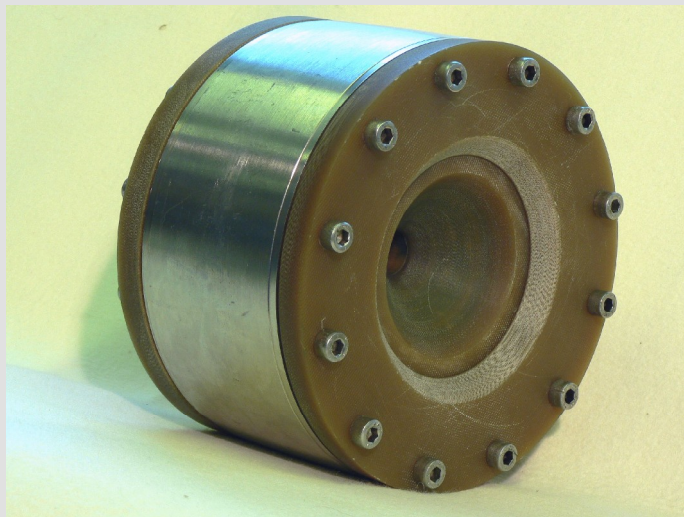


New magnet coil

- coil is wound of CuNbTi wire
- bore of 20 mm \varnothing , external $\varnothing = 130$ mm, height = 80 mm
- $R(T=77K) = 60$ m Ω
- Opening angle of the coil: 40°
- coil is horizontally mounted
- $B //$ beam (Faraday geometry)
- magnet immersed in liquid nitrogen

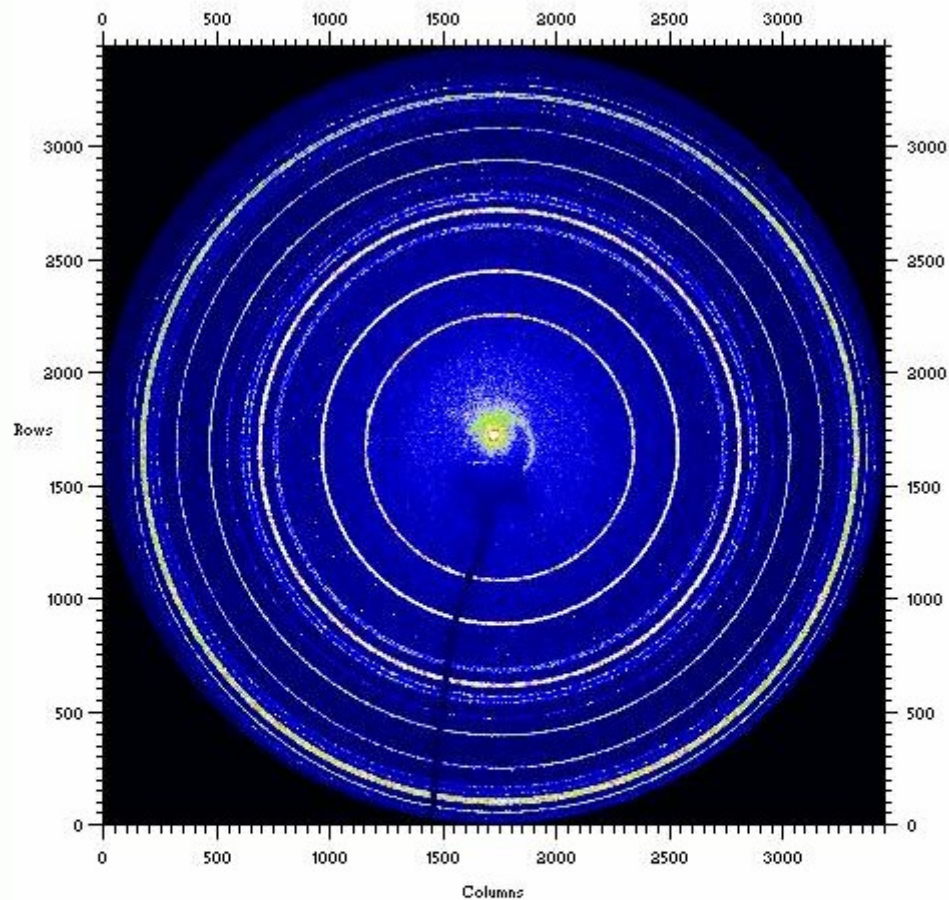
New N₂ cryostat

- 2 Kapton foils (120 μ m thickness)
- Optical access angles: up to 31°/36°



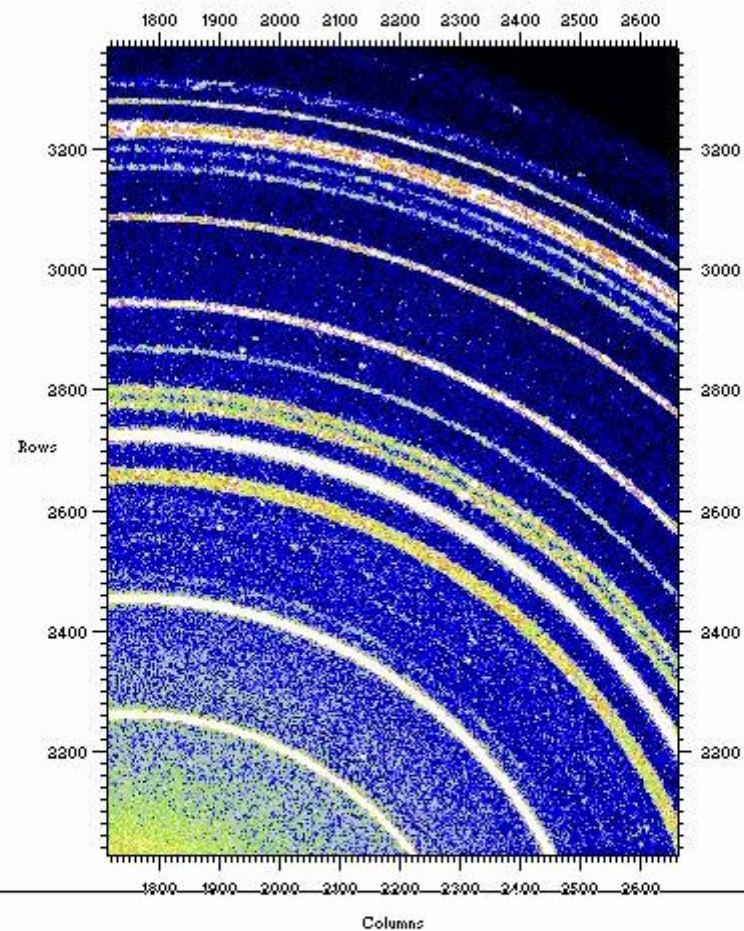
Light Graphics Window

D:\HMF_RX\Mesures_ESRF\HE2788_ID20Nov2006\TbVO_10-11-06\TbVO_030.mar3450



Light Graphics Window

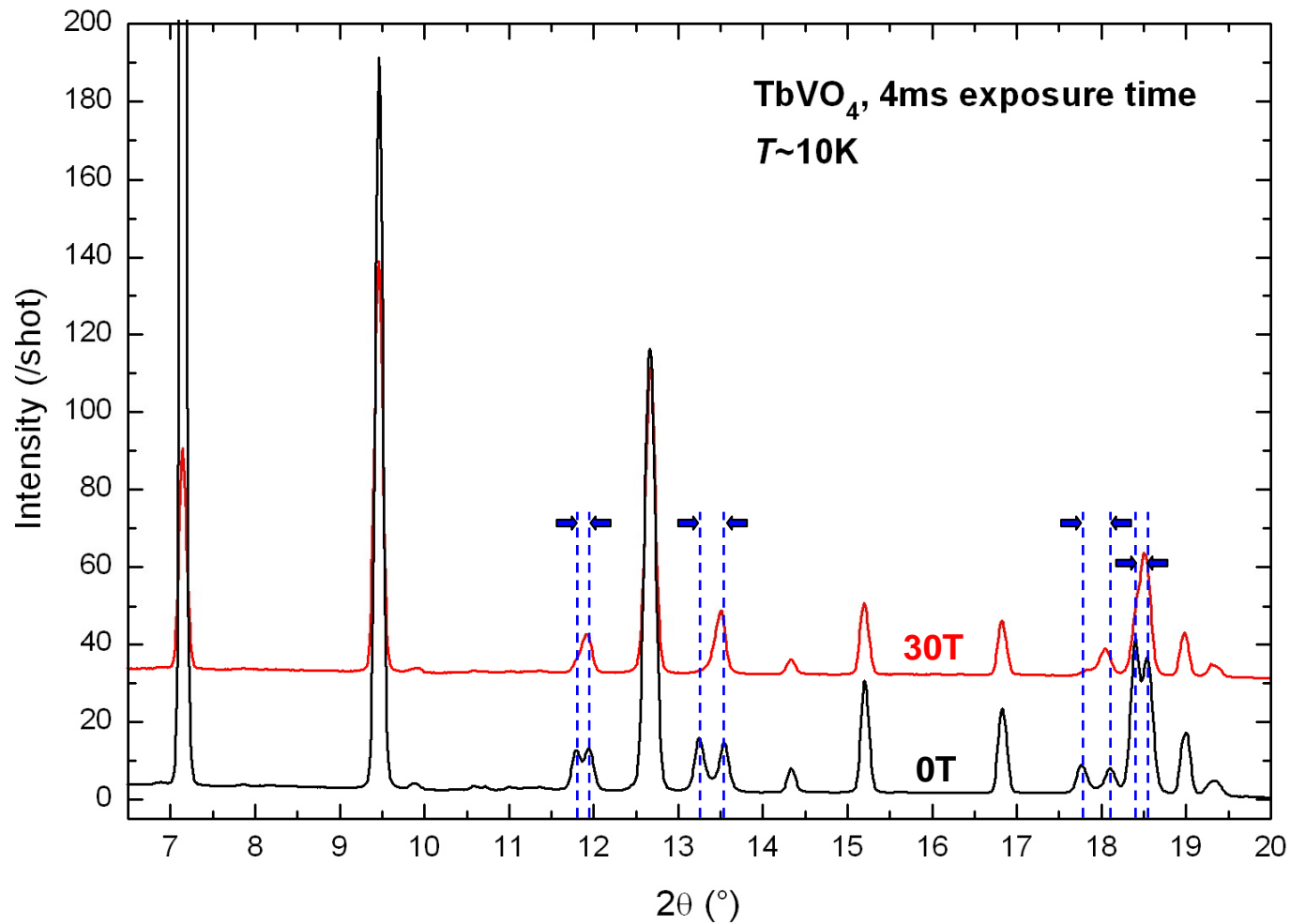
D:\HMF_RX\Mesures_ESRF\HE2788_ID20Nov2006\TbVO_10-11-06\TbVO_030.mar3450



EXIT	BEAM CENTRE	FULL	OUTPUT
?	CAKE	INPUT	NORMALISE
HELP	PROJECTION	INTEGRATE	Z-SCALING
PRINT	EXCHANGE	MASK	ZOOM IN
DISPLAY	OPTIONS	1-D TRANSFORMS	IN-ZOOM

EXIT	BEAM CENTRE	FULL	OUTPUT
?	CAKE	INPUT	NORMALISE
HELP	PROJECTION	INTEGRATE	Z-SCALING
PRINT	EXCHANGE	MASK	ZOOM IN
DISPLAY	OPTIONS	1-D TRANSFORMS	IN-ZOOM

Diffraction pattern on TbVO_4



Future applications

- Mobile experimental device, can be used on a non-dedicated beamline (ESRF, SOLEIL)
- Other X-ray techniques: Spectroscopy (EXAFS, XMCD)
Powder and single crystal diffraction (Laue Diffraction)
- Field induced magneto-structural transitions: magneto-caloric compounds, manganites, multiferroïcs, frustrated systems, superconductors, metamagnetic transitions, etc ...

New beamline at the ESRF: ID06 will become operational at the end of 2007

ANR project: SysMAF (2006-2008)

Diffraction et Spectroscopie des rayons X synchrotron sous champ magnétique intense



Post-doctoral position available at the LNCMP

- NWO/FWO Vlaanderen and ESRF : beamtime allocation
- DUBBLE CRG staff : F. Meneau, D. Detollenaere, J. Jacobs
- ESRF Safety group
- P. Van der Linden : cryogenics support
- ESRF detector pool and T. Buslaps (ESRF, ID15 beamline) : X-ray detector
- P.C. Canfield (Ames Laboratory, Ames, IA) : TbVO₄ samples

Thank you for your attention !